Nonlinear Modeling by Assembling Piecewise Linear Models

Weigang Yao[1] and Meng-Sing Liou[2]
NASA John H. Glenn Research Center at Lewis Field, Cleveland, Ohio 44135

To preserve nonlinearity of a full order system over a parameters range of interest, we propose a simple modeling approach by assembling a set of piecewise local solutions, including the first-order Taylor series terms expanded about some sampling states. The work by Rewienski and White [1] inspired our use of piecewise linear local solutions. The assembly of these local approximations is accomplished by assigning nonlinear weights, through radial basis functions in this study. The efficacy of the proposed procedure is validated for a two-dimensional airfoil moving at different Mach numbers and pitching motions, under which the flow exhibits prominent nonlinear behaviors. All results confirm that our nonlinear model is accurate and stable for predicting not only aerodynamic forces but also detailed flowfields. Moreover, the model is robustness—accurate for inputs considerably different from the base trajectory in form and magnitude. This modeling preserves nonlinearity of the problems considered in a rather simple and accurate manner.

I. Introduction

Aerodynamics problems are highly nonlinear and are routinely solved nowadays by computational fluid dynamics methods through validated computer codes, thanks to the availability of fast-improving computer technologies. However, the need for striving to reduce the computation time has become as strong, if not more, as ever because more details (thus more grid points and higher fidelity) are demanded and coupling of disciplines (such as structure, control, chemistry, etc.) required for considering an engineering system. Furthermore, optimization problems require repeated computations of similar setup, but with variations in design variables that may have a large variation in values. Thus, there exists a strong desire to replace the original full model with an approximate model that is much computational intensive. This may be achieved in several ways, such as model order reduction whose concept is to find an approximation with number of unknowns much smaller than the full system. Or one can base on a set of available data (empirical or CFD solutions), valid at discrete parametric conditions, to build a model that presumably will be valid inside the parameters (state) range but also beyond to some extent. The latter is typically employed in surrogate modeling, metamodeling, and the like. Notwithstanding, the key question (hence criterion) is that the fidelity of the original model must be preserved to the extent necessary. This requirement broadly translates into the preservation of nonlinear behavior in aerodynamics. This is the goal of the research reported here: modeling for efficiency and accuracy.

Our research into model reduction has been motivated by the need for performing multidisciplinary analysis and optimization for an aeronautical system under the current Fundamental Aeronautics Program. In particular, aeroelasticity is the subject of interest—we are concerned with the coupling of unsteady aerodynamics and structure dynamics and its interactive effects, specially the limit cycle oscillations (LCO). For which, numerous scenarios must be evaluated to relate the output in response to the input parameters.

Conventional aeroelastic stability analysis is often formulated simply in terms of an input-output relationship, where input is aerodynamic force and output is structural response. System identification (ID) method is a straightforward framework to construct a simple yet theoretically rigorous reduced order model (ROM) at the expense of detailed flowfield information. For example, such flow flied characteristic will be required to find a new aerodynamic shape to minimize occurrence of structure flutter in an aeroelastic optimization problem.

---

[1] Research Associate, NASA Postdoc Program; Currently Visiting Scholar, Western Michigan Uinversity, Kalamazoo, MI 49008; member AIAA.
[2] Senior Technologist; Associate Fellow AIAA.

To retain flowfield details, the state-space project method based on modes superimposition has often been employed. Unfortunately, the linear superimposition of modes limits the method from describing nonlinear phenomenon such as limit cycle oscillations.

The basic concept of State-Space Projection method is to find a subspace or transformation matrix, onto which the full order system can be projected with a much smaller dimension. A well-known method to define such subspace is proper orthogonal decomposition (POD). Beran et al. [2] have used the POD method to construct ROM of aeroelastic system. A key ingredient of POD is to collect snapshots of the time-dependent solution. Once the snapshot matrix is formed, the subspace can be derived from an eigenvalue analysis. Traditional POD method merely takes input characteristics into account. Moore [3] introduced the Balance Truncation (BT) method to define the subspace by including both the input and output characteristics of the full order system. As a result, the BT method often yields not only more accurate but also lower order ROM than POD. Laub [4] proposed a more efficient way to derive the transformation vector. Willcox and Peraire [5] and Rowely [6] respectively applied POD snapshot ideas to extend the original BT method to study fluid dynamics problems.

Linear or nonlinear full order model representation is required for current POD/snapshot-BT method. It is relatively straightforward to obtain a *linear* model of a highly nonlinear system by retaining the first-order terms; this is simply done, for example, by finite differencing a CFD code. However, it remains challenging to obtain a *nonlinear* model of the CFD code, as elaborated below. Let us consider a time-dependent nonlinear system,

$$\dot{\boldsymbol{x}} = f(\boldsymbol{x}, \boldsymbol{u}) \tag{1}$$

where $\boldsymbol{x}$ is a $N\times1$ state vector; $\boldsymbol{u}$ a $P\times1$ input vector. An appropriate projection can be chosen to construct a nonlinear ROM in a subspace $\boldsymbol{\phi}$, expressed as:

$$\dot{\boldsymbol{x}}_r = \boldsymbol{\phi}^T f(\boldsymbol{\phi} \cdot \boldsymbol{x}_r, \boldsymbol{u}) \tag{2}$$

where $\boldsymbol{x}_r$ is a $R\times1$ state vector, with $R << N$. An intuitive way of arriving at a nonlinear representation is to include the second-order terms in the Taylor's series expansion, thus involving the Hessian matrix of f. However, it renders computationally intractable to obtain the Hessian matrix for a fluid system in CFD.

Rewienski and White[1] introduced a trajectory piecewise-linear (TPWL) approach for constructing a nonlinear model: including the projections of state variables and the governing nonlinear differential equations onto a subspace and a proper weighting of a number of these truncated linear models expanded about some operating points (or called sample states in this paper as in [7]) along the state trajectory. Gu and Roychowdhury [7] proposed a similar but distinguishably different technique and demonstrated its advantages over the TPWL. Gratton and Wilcox [8] combined the TPWL and POD methods to derive a reduced model to study a flow control scheme for supersonic diffuser. Jesmani et al [9], taking advantage of linear characteristics of flow in streamline coordinates, applied the TPWL for prediction of pressure and water saturation in oil reservoirs.

Previously, we presented the idea of assembling a number of weighted neurons associated with different inputs to arrive at a nonlinear reduced model via recurrent artificial neural network training [10] in which the weights are based on the radial basis functions. This thinking follows the general concept of metamodeling. The present work extends the similar concept for constructing a nonlinear model by collecting a set of submodels that are each valid in the neighborhood of sample points. The idea of TPWL comes handy so that we can simply replace the neurons with the piecewise linear solutions valid around the sample points. It is expected that including the first-order Taylor expansion terms will enhance the "ball" of validity, consequently the resulting model should be more robust.

The objective of our work is to ultimately establish an accurate, stable, and efficient procedure to construct a nonlinear model that can be used reliably to describe nonlinear behavior in an aeroelasticity system; this paper presents the first installment towards that objective. Major efficiency gains will come in an upcoming paper in which the balanced truncation technique is implemented to reduce the order of the approximate system. The present paper is organized as follows. First, the basic concept of piecewise linearization (PWL) in a state trajectory is presented for a simple nonlinear scalar equation to illustrate how the PWL-based approximate model

works. Section III gives the details for constructing a nonlinear model from CFD solutions. Validation of the so-constructed model is shown in Section V and VI, using the AGARD test cases, CT5 and CT2 [13], as a baseline. Key issues to its construction are discussed in Section VI, with additional results attesting the efficacy of the proposed modeling approach. Finally, we summarize the paper and outline future plan for continuing the work.

II. Piecewise-Linearization

In this section the basic idea of piecewise linear approximation is outlined, while the interested reader should consult [1] for details. Applying the first order Taylor expansion of the nonlinear system Eq. (1) around sample points $(\boldsymbol{x}_1, \boldsymbol{u}_1)$, $(\boldsymbol{x}_2, \boldsymbol{u}_2)$ … $(\boldsymbol{x}_p, \boldsymbol{u}_p)$ gives

$$\begin{cases} \dot{\boldsymbol{x}} \approx f(\boldsymbol{x}_1,\boldsymbol{u}_1)+\dfrac{\partial \boldsymbol{f}}{\partial \boldsymbol{x}}\cdot\left(\boldsymbol{x}-\boldsymbol{x}_1\right)+\dfrac{\partial \boldsymbol{f}}{\partial \boldsymbol{u}}\cdot\left(\boldsymbol{u}-\boldsymbol{u}_1\right) \\ \dot{\boldsymbol{x}} \approx f(\boldsymbol{x}_2,\boldsymbol{u}_2)+\dfrac{\partial \boldsymbol{f}}{\partial \boldsymbol{x}}\cdot\left(\boldsymbol{x}-\boldsymbol{x}_2\right)+\dfrac{\partial \boldsymbol{f}}{\partial \boldsymbol{u}}\cdot\left(\boldsymbol{u}-\boldsymbol{u}_2\right) \\ \vdots \\ \dot{\boldsymbol{x}} \approx f(\boldsymbol{x}_p,\boldsymbol{u}_p)+\dfrac{\partial \boldsymbol{f}}{\partial \boldsymbol{x}}\cdot\left(\boldsymbol{x}-\boldsymbol{x}_p\right)+\dfrac{\partial \boldsymbol{f}}{\partial \boldsymbol{u}}\cdot\left(\boldsymbol{u}-\boldsymbol{u}_p\right) \end{cases} \tag{3}$$

Each of the above expansion is assumed to have an adequate range of validity in the neighborhood of its sample point. It is anticipated that a proper assemblage of these piecewise linear approximation will provide an approximation over an enlarged domain and a nonlinear combination of them will potentially preserve the nonlinearity of the original nonlinear system. Introducing a nonlinear weight w_i to each piecewise linear approximation near $(\boldsymbol{x}_i, \boldsymbol{u}_i)$ to form a weighted sum of Eq. (3),

$$\dot{\boldsymbol{x}} \approx \sum_{i=1}^{p} w_i \cdot \left(f(\boldsymbol{x}_i,\boldsymbol{u}_i)+\left.\frac{\partial \boldsymbol{f}}{\partial \boldsymbol{x}}\right|_{x=x_i}\cdot\left(\boldsymbol{x}-\boldsymbol{x}_i\right)+\left.\frac{\partial \boldsymbol{f}}{\partial \boldsymbol{u}}\right|_{u=u_i}\cdot\left(\boldsymbol{u}-\boldsymbol{u}_i\right)\right) \tag{4}$$

where the weights satisfy,

$$\sum_{i=1}^{p} w_i = 1 \tag{5}$$

Eq. (5) can be rewritten, using the Jacobians of $\boldsymbol{f}$ with respect to state variable $\boldsymbol{x}$ and input variable $\boldsymbol{u}$, as

$$\begin{gathered} \dot{\boldsymbol{x}} \approx \sum_{i=1}^{p} w_i \cdot \left(f(\boldsymbol{x}_i,\boldsymbol{u}_i) + A_i \cdot \left(\boldsymbol{x}-\boldsymbol{x}_i\right) + B_i \cdot \left(\boldsymbol{u}-\boldsymbol{u}_i\right)\right) \\ A_i = \left.\frac{\partial \boldsymbol{f}}{\partial \boldsymbol{x}}\right|_{x=x_i}, B_i = \left.\frac{\partial \boldsymbol{f}}{\partial \boldsymbol{u}}\right|_{u=u_i} \end{gathered} \tag{6}$$

This provides us a framework to represent the nonlinear model Eq. (1) with a combination of linear model, with three questions to be answered: (1) How many sample points (p) are necessary? (2) How are the sample points distributed? and (3) How are the weight functions determined? We are not aware of any rigorous and general rules addressing these issues and suspect that one may likely rely on experiences on practicing and verification and need to have good understanding of the physical problems under consideration. Nevertheless, some rules and knowledge, albeit problem dependent, will be accumulated, thus providing a useful guide. The first two questions will be evaluated quantitatively in the present study. The third one has been studied in the general context of surrogate model [11]. Here, we shall adopt the radial basis function (RBF) of the Euclid distance between the state $\boldsymbol{x}$ and the sample (operating) point, also used in [10],

$$w_i(x) = e^{-\frac{\|x-x_i\|}{\delta_i^2}} \Big/ \sum_{j=1}^{p} e^{-\frac{\|x-x_j\|}{\delta_j^2}} \tag{7}$$

where $\| x\text{-}x_i \|$ is the L2-norm (Euclidean distance) of the vector $x\text{-}x_i$, x_i is the sample state, δ_i is the width parameter. In this paper we take $\delta_k = 1/\sqrt{50}$ for all CFD calculations. Schematically the nonlinear model can be viewed as in Figure **1**.

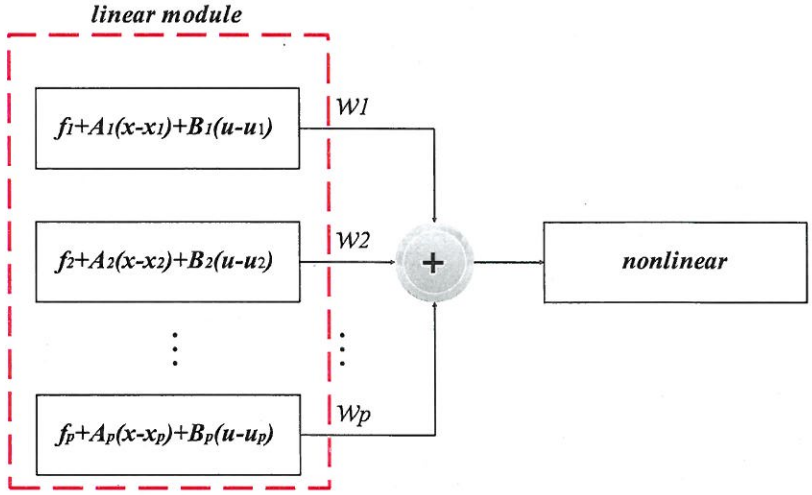

Figure 1. Assembly of piecewise linear module to form an approximate nonlinear system. General Guidelines.

A. Validation of the Piecewise Linear (PWL) Model

In order to evaluate the validity of the above piecewise linear concept for a nonlinear system, a simple model is considered,

$$\dot{x} = f(x,u) = 5 \cdot \sin x + x + u \tag{8}$$

According to Eq. (4), the nonlinear system Eq. (8) is approximated as,

$$\dot{x} = f(x,u) = 5 \cdot \sin x + x + u \approx \sum_{i=1}^{p} w_i \cdot \left(f_0 + a_i \cdot \left(x - x_i \right) + b_i \cdot \left(u - u_i \right) \right) \tag{9}$$

Here, the notation a_i and b_i is used to replace Jacobian $\boldsymbol{A_i}$, $\boldsymbol{B_i}$, since the number of states of the model is one. These derivatives a_i and b_i are available analytically

$$\begin{cases} \left. \dfrac{\partial f}{\partial x} \right|_{x=x_i} = 5 \cdot \cos x_i + 1 \\ \left. \dfrac{\partial f}{\partial u} \right|_{u=u_i} = 1 \end{cases} \tag{10}$$

Obviously, accuracy of Eq. (9) highly depends on the choice of sample points (x_i, u_i) at which the training of input-output relationship will be imbedded in the model. The training signal can be determined according to the range of interest. Here, the input signal is defined as,

$$u = \sin(6t) + \cos(6t) \tag{11}$$

With the initial condition $x_1 = 0$ and input signal Eq. (11), the output of Eq. (8) can be numerically integrated by using the standard 4-stage Runge-Kutta method for time integration and is shown in Figure 2.

A total of 30 sample states x were chosen uniformly to build the piecewise linear model, Eq. (9), with the first and last sample points set at $t = 0$, and $t = 3.0$ respectively. Figure 3. is the output of the PWL model with different

numbers of PWL models: one PWL is only valid around the first sample point as expected. Using the error between the "exact" output ($\hat{x}$) and the PWL model

$$Error = \frac{100 \times \frac{1}{N} \sum_{i=1}^{N} |\hat{x}_i - x_i|}{x_{\max} - x_{\min}} \tag{12}$$

allows us to evaluate the effects of the size (p) of PWL models.

As shown in Table. 1, the error decreases as the number of PWL increases. Eventually, a 3-PWL model was chosen to form a representation of the nonlinear system Eq. (8) since p = 5 offers only an additional 0.12% reduction in error. As stated above, the PWL was obtained by training the nonlinear system Eq. (8) with the signal Eq. (11) for t∈[0, 3.0]. To see the usefulness (or robustness) of this approximation, it is necessary to evaluate the model's performance at t > 3.0(s) or with different signal input. Figure 4. is the output using the 3-PWL derived before, in comparison with the solution of the full nonlinear system. The 3-PWL remains accurate for t > 3.0(s). This is not entirely unexpected because the state variation after t > 3.0(s) still falls in the range of $x(t)$ for $t < 3.0$, but nonetheless confirming that the model also adjusts to the asymptotic periodic solution after the transient period. Next, we test a very different input signal

$$u = \sin^3(6t) \tag{13}$$

Figure **5**. shows that the same 3-PWL still gives an accurate output. However, it is worth reminding that the reliability of the model strongly depends on the training data, namely the sample points; some judicious choice of training trajectory is useful for maintaining the model's range of validity.

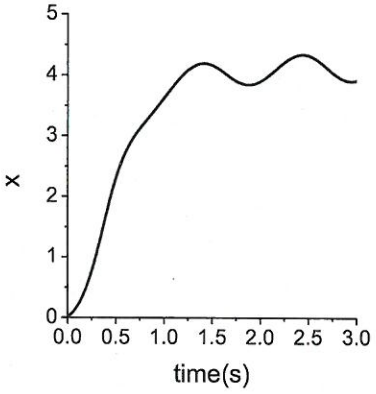

Figure 2. Output of system Eq. (8).

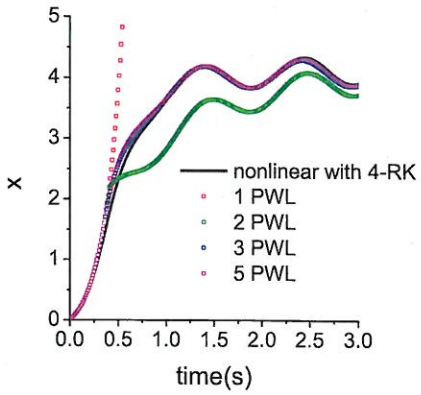

Figure 3. Output of PWL model.

Table. 1 Error of different PWL No.

PWL No.	Error (%)
2	8.69
3	1.19
5	1.07

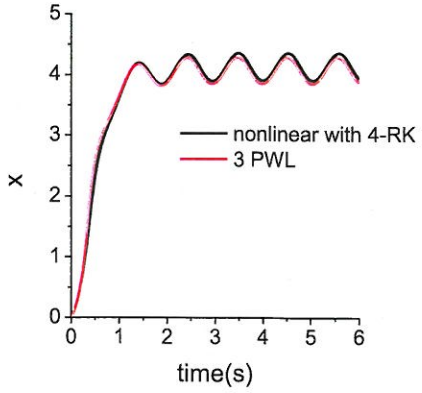

Figure 4. output at t > 3.0(s).

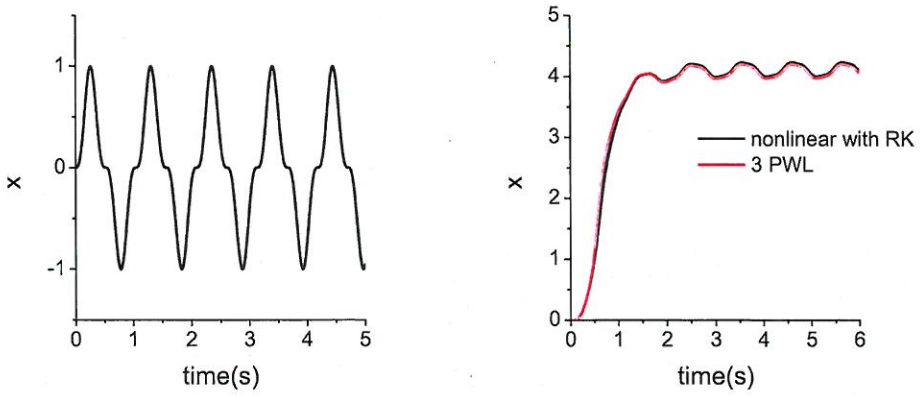

(a) Input signal. **(b) Output comparison.**

Figure 5. results with input signal (13).

III. CFD modeling by Piecewise Linear Construction

A 2D inviscid CFD solver is used here to demonstrate how to construct a CFD-based PWL model. From the aeroelasticity viewpoint the output of CFD is aerodynamic forces, which often exhibit nonlinear behavior with respect to inputs, such as motion or shape change of a wing. Without loss of generality, the inviscid CFD equations can be written as,

$$\frac{\partial(\upsilon \mathbf{q})}{\partial t} = \mathbf{R}(\mathbf{q},\mathbf{u},\mathbf{v}) \tag{14}$$

Where υ is the volume of a computational cell, $\mathbf{q}$ consists of conservative flow variables, $\mathbf{R(q,u,v)}$ is the residual describing derivatives of flow flux functions, for a set of input conditions, $\mathbf{u}$ and $\mathbf{v}$, which are the structure displacement and velocity respectively for the cases considered in this paper. The spatial discretization contained in the residual term $\mathbf{R(Q)}$ can be determined by a state-of-the-art numerical flux method; here we employ the AUSM$^+$-up scheme [12] for the flux function together with the van Albada limiter in the MUSCL interpolation of primitive variables. The time integration is done by using the 4-stage Runge-Kutta method together with a dual-time iterative scheme incorporated to ensure that the accuracy of the time-discrete form of unsteady equations be preserved at each time step.

Now for the model system, we follow the same procedure described in Eqs. (3-5). The residual term $\mathbf{R(q,u,v)}$ in Eq. (14) may be approximated with a collection of the first-order Taylor series terms expanded about a set of appropriately defined sample points, $\mathbf{Q}_i = (\mathbf{q}_i, \mathbf{u}_i, \mathbf{v}_i)$, $i = 1,\ldots, p$. Expanding $\mathbf{R(q,u,v)}$ about a sample state $\mathbf{Q}_i$, we get

$$\begin{aligned} \mathbf{R}(\mathbf{Q}) &= \mathbf{R}(\mathbf{Q}_i) + \mathbf{A}_i(\mathbf{q}-\mathbf{q}_i) + \mathbf{B}_{1,i}(\mathbf{u}-\mathbf{u}_i) + \mathbf{B}_{2,i}(\mathbf{v}-\mathbf{v}_i) + \ldots \\ \mathbf{A}_i &= \left.\frac{\partial \mathbf{R}}{\partial \mathbf{q}}\right|_i, \quad \mathbf{B}_{1,i} = \left.\frac{\partial \mathbf{R}}{\partial \mathbf{u}}\right|_i, \quad \mathbf{B}_{2,i} = \left.\frac{\partial \mathbf{R}}{\partial \mathbf{v}}\right|_i \end{aligned} \tag{15}$$

where the Jacobians of $\mathbf{R(q,u,v)}$ with respect to its arguments are $\mathbf{A}$, $\mathbf{B}_1$ and $\mathbf{B}_2$ respectively. Hence, Eq. (14) becomes,

$$\frac{\partial(\upsilon\mathbf{q})}{\partial t}=\sum_{i=1}^{p}w_i(\mathbf{Q},\mathbf{Q}_i)\left(\mathbf{R}(\mathbf{Q}_i)+\mathbf{A}_i\left(\mathbf{q}-\mathbf{q}_i\right)+\mathbf{B}_{1,i}\left(\mathbf{u}-\mathbf{u}_i\right)+\mathbf{B}_{2,i}\left(\mathbf{v}-\mathbf{v}_i\right)\right) \tag{16}$$

The right-hand term of Eq. (16) is a weighted combination of locally linearized models; it is completely linearized except the weighting functions. The solution of this system is computationally tractable, bypassing the need of flux evaluations for the entire flow domain and requiring only matrix-vector multiplications besides evaluating the weights. In this study, the same procedure used in the full model for time integration is again used here. It is worth noting that in this formulation, the grid motion expressed in terms of υ need be computed as well, via either a prescribed motion or an implicitly coupled system as in the case of flexible wing whose deformation is affected by and changes the flow simultaneously.

Assuming a continuous grid motion, the time derivative can be further rearranged, by knowing the volume υ is a function of airfoil displacement $\mathbf{u}$ and velocity $\mathbf{v} = \partial\mathbf{u}/\partial t$,

$$\frac{\partial}{\partial t}\left(\upsilon\mathbf{q}\right)\approx(\mathbf{q}\frac{\partial\upsilon}{\partial\mathbf{u}})_i\mathbf{v}+\upsilon_i\frac{\partial\mathbf{q}}{\partial t}=\mathbf{C}_i\mathbf{v}+\upsilon_i\frac{\partial\mathbf{q}}{\partial t} \tag{17}$$

Substitute Eq. (17) into Eq. (16),

$$\frac{\partial\mathbf{q}}{\partial t}=\sum_{i=1}^{p}\frac{w_i}{\upsilon_i}\left(\mathbf{R}(\mathbf{Q}_i)+\mathbf{A}_i\left(\mathbf{q}-\mathbf{q}_i\right)+\mathbf{B}_{1,i}\left(\mathbf{u}-\mathbf{u}_i\right)+\mathbf{B}_{2,i}\left(\mathbf{v}-\mathbf{v}_i\right)-\mathbf{C}_i\mathbf{v}\right) \tag{18}$$

Now the grid motion is explicitly folded in the right-hand-side term through the Jacobian matrix **C;** all that is required boils down to the time evolution of the state vector **q.** As we consider only rigid body motion in this study, this is the equation used. Thus, the following dual-time iterative system is solved for the increment of **q** in each time increment of the 4-stage Runge-Kutta method,

$$\frac{\mathbf{q}_{m+1}-\mathbf{q}_m}{\Delta\tau}+\frac{\mathbf{q}_m-\mathbf{q}_n}{\Delta t}=\sum_{i=1}^{p}\frac{w_i}{\upsilon_i}\left(\mathbf{R}(\mathbf{Q}_i)+\mathbf{A}_i\left(\mathbf{q}-\mathbf{q}_i\right)+\mathbf{B}_{1,i}\left(\mathbf{u}-\mathbf{u}_i\right)+\mathbf{B}_{2,i}\left(\mathbf{v}-\mathbf{v}_i\right)-\mathbf{C}_i\mathbf{v}\right) \tag{19}$$

where the subscript "m" denotes the iterative index for the dual time and subscript "n" for the physical time. The fictitious step used in the dual time $\Delta\tau$ is calculated by,

$$\Delta\tau=\sum_{i=1}^{p}w_i\Delta t_{local,i} \tag{20}$$

Solving Eq. (19) does not require tracking of grid deformation, the grid motion is already included in $\mathbf{C}_i\mathbf{v}$. However, aerodynamic force is still obtained by integrating the pressure force over the instantaneous position of the moving body. The grid information should be updated at each physical time step. For a 2D problem, like the cases studied in this paper, the computational time for grid deformation is negligible and so is the integration of forces over the body. However, by skipping a direct integration of forces over the body at each time step, it is consistent, to the order of accuracy involved in the above weighted combination of piecewise linear expansions, to express the aerodynamic forces in the form of the first-order Taylor expansion of the aerodynamic force about each sample point,

$$\mathbf{F}\approx\mathbf{F}_i+\left.\frac{\partial\mathbf{F}}{\partial\mathbf{q}}\right|_i\left(\mathbf{q}-\mathbf{q}_i\right) \tag{21}$$

Then, the PWL model for the aerodynamic force is formulated similarly using the same set of sample points and weighting functions.

$$\mathbf{F}\approx\sum_{i=1}^{p}w_i\mathbf{F}_i+\sum_{i=1}^{p}w_i\left.\frac{\partial\boldsymbol{F}}{\partial\mathbf{q}}\right|_i\left(\mathbf{q}-\sum_{i=1}^{p}\mathbf{q}_i\right) \tag{22}$$

All three procedures have been implemented to compute the aerodynamic forces and they do not give rise to noticeable differences, hence not shown in the present paper. The aerodynamic force shown in the remainder of the paper is computed through Eq. (22).

IV. Validation of Nonlinear CFD Model

In order to demonstrate the validity and performance of the above-constructed CFD PWL-based nonlinear model, a 2D NACA 0012 airfoil in pitching motion will be used for various flow conditions that result in vastly different aerodynamic behaviors. Special interest is paid to the nonlinear characteristics. In the present study, we are exclusively interested in unsteady aerodynamic characteristics where the inviscid mechanism plays the dominant role. In order to confirm the baseline solution, some standard test cases put forth in the AGARD report [13] will be used, specifically the so-called CT2 and CT5 cases. These two cases have different flight Mach numbers and pitching parameters, as summarized in Table 2. The pitching motion of the airfoil is described by its angle of attack changing in time

$$\alpha(t) = \alpha_m + \alpha_0 \sin(\omega t) = \alpha_m + \alpha_0 \sin(2k\tilde{t}), \quad k = \frac{\omega c}{2U_\infty}, \quad \tilde{t} = \frac{tU_\infty}{c} \tag{23}$$

where k is the reduced frequency defined by the free stream velocity U_∞ and the chord length c, and the pitching centers at x_m, given in Table.2 as well.

Table. 2 Parameters of CT2 and CT5 cases

Case	M_∞	α_m	α_0	k	x_m
CT2	0.6	3.16°	4.59	0.0811	0.273
CT5	0.755	0.016°	2.51	0.0814	0.25

Since the inviscid force is the primary controlling mechanism for the unsteady aerodynamic characteristics of interest, an O-type grid around the airfoil is appropriate for the CFD computation. A grid of 61×21 points (in radial and circumferential directions respectively) is generated, as shown in

Figure **6**. This results in a state vector **q** with a size of 4800 (60×20×4, where a CFD solution vector for a 2D problem has 4 components [ρ, ρu, ρv, ρE] for each computational cell.)

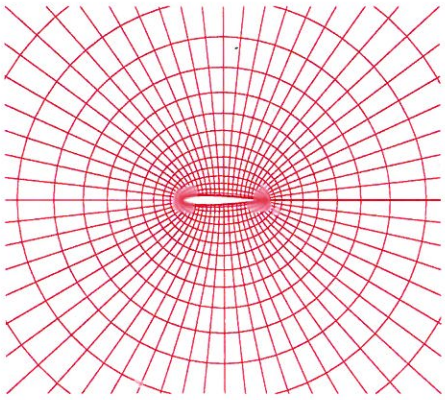

Figure 6. Inviscid grid around the NACA 0012 airfoil.

First, we validated the accuracy of the CFD procedure against the experimental data reported in [13]; the comparison of aerodynamic forces in a cycle for both the CT2 and CT5 cases is given in Figure 7. and Figure 8. respectively, showing the CFD results in good agreement with the data. More importantly, both test cases exhibit a strong nonlinear behavior in the moment coefficient and nonsymmetrical forces between downward and upward motions. It is noted that CT2 has a significantly larger excursion in pitching than CT5, thus it is expected to show stronger nonlinear effects. On the other hand, CT5 operates at a higher Mach number, and it is anticipated to have a supersonic pocket in the flowfield during certain phase of the pitching.

This validation establishes a solid foundation for trusting the solutions at any point along the pitching trajectory; that is, any point is equally legitimate to be chosen, insofar as its accuracy is concerned, as a sample solution--a piecewise linear model in this case. In the remainder of this paper, we shall focus on the performance of the nonlinear model built from such PWL solutions (submodels).

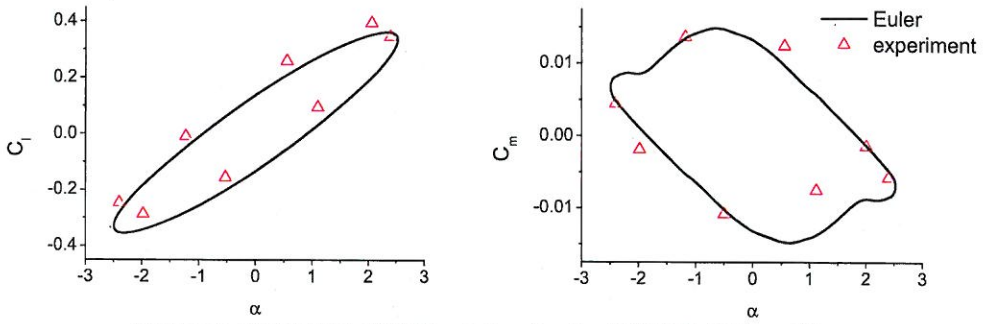

Figure 7. Validation of CFD solution for the AGARD CT5 problem.

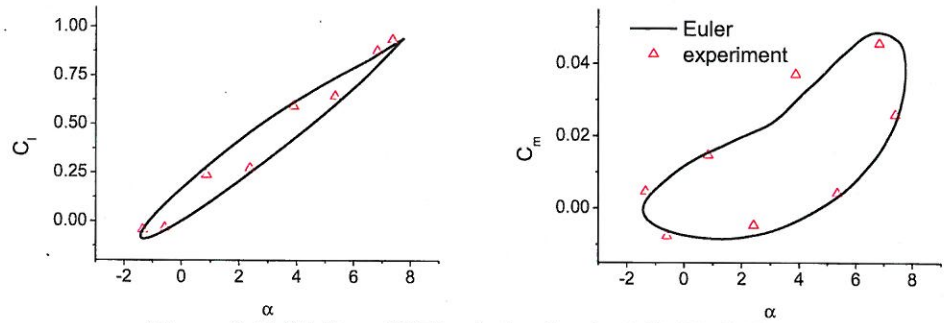

Figure 8. Validation of CFD solution for the AGARD CT2 problem.

V. Practical Issues about Constructing the Nonlinear Model

As mentioned previously, the training dataset, i.e. the piecewise linear solutions, must be representative, containing essential flow characteristics, so that the final overall model can be useful for a range sufficiently far away from the baseline trajectory to cover a wide range of input parameters. The number of sample points should not be too "large" so that the computational effort is practical and the distribution of these points should not be too "specific" so that no *a priori* knowledge about the flow details is necessary. However, some intuitive judicious judgment may be helpful.

A. Effect of Sampling

To our knowledge, there are no intelligent and general criteria to pre-determine a better set of sample points. We simply base on the time coordinate, instead of following the flight trajectory of angle of attack. During a pitching period T, the physical time step for time integration is divided into 60 equal time steps, i.e., $\Delta t = T/60$. Out of these 60 time slices, 20 equally-spaced sample points are chosen, at which the PWL solutions, hence denoted as PWL(20), are gathered, as shown in Figure 9. for the CT5 problem. For constructing the CT5 model, we used $\alpha_0 = 3.5^\circ$ as the baseline training. To test the effect of the number of PWL solution, we also used 13 sample points, clustered around the extreme points of the motion; the solutions, called PWL(13), are included in Figure 10. for comparison with the full CFD and the PWL20 solutions; again both the PWL-based solutions agree closely with the CFD solution, as shown in

Figure **11**, also for other two flight trajectories with $\alpha_0 = 3.0^\circ$ and 2.5°. There does not appear a definitive trend to judge whether PWL(20) performs better than PWL(13), however the latter certainly requires much less computational efforts. As a result, this does suggest a more intelligent way (in this case clustering sample points near the peak angles) can be more effective.

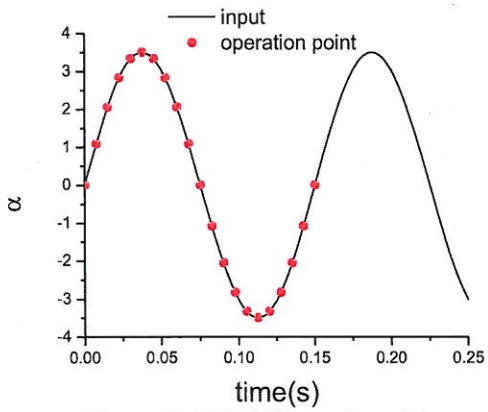

Figure 9. PWL(20) sample points.

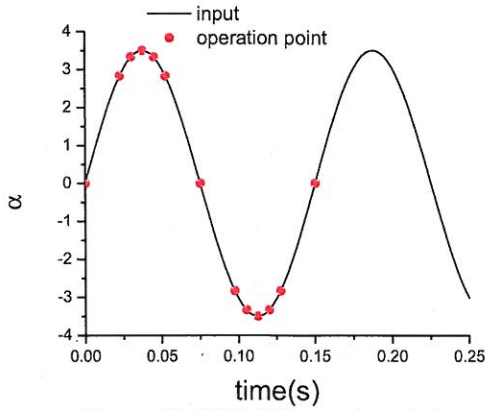

Figure 10. PWL(13) sample points.

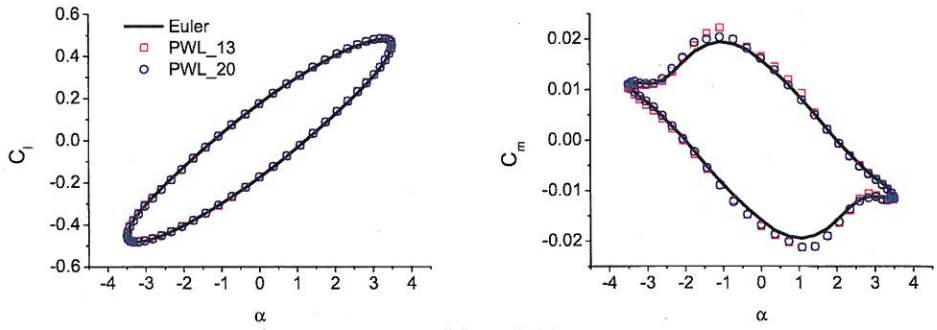

(a) $\alpha_0 = 3.5^\circ$.

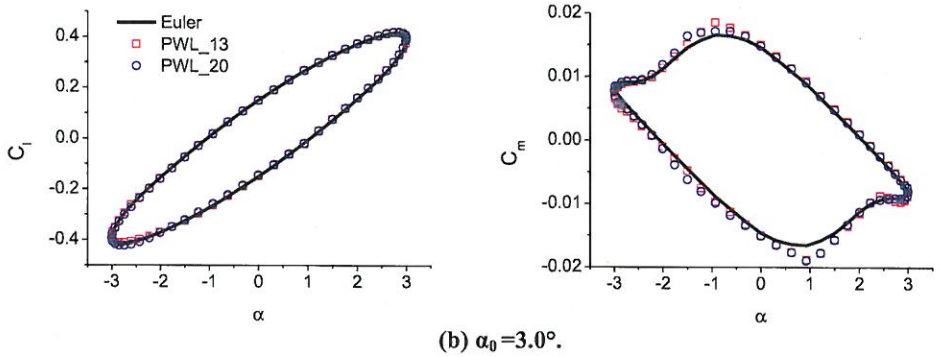

(b) α_0=3.0°.

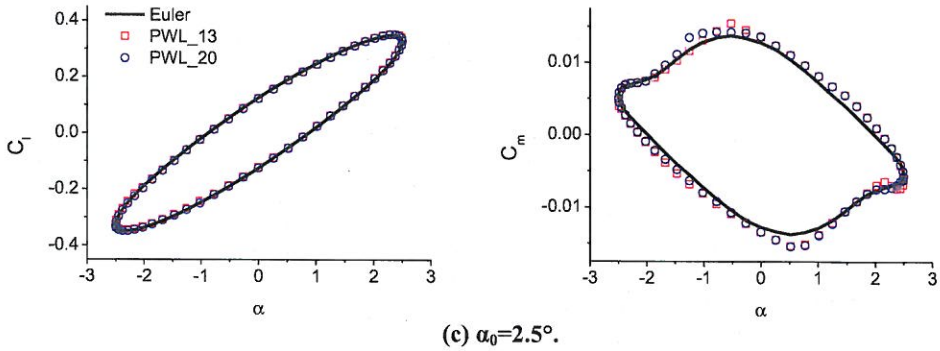

(c) α_0=2.5°.

Figure 11. Effect of distribution of sample points on CT5 solutions: nonuniformly-spaced (PWL(13)) vs. uniformly spaced (PWL(20)) points.

Shown in

Figure **12**. are the results of the full CFD model and the nonlinear model using 30, 20 and 10 PWL solutions for CT5 at $\alpha_0 = 3.5°$, suggesting that both 20 and 10 PWL models can faithfully capture nonlinear features of the original CFD system as well. On the other hand, the linear results, obtained by retaining only the 1st order Taylor expansion around the steady operation point, which is at the time $t = 0$(s), completely misses the nonlinear phenomenon in the original system. It is noted that the linear model is commonly used to generate linear model of CFD system for order reduction. As the linear model does not contain any time varying information in the model, it becomes clear collecting time-varying submodels into the model is a very essential element and a key to maintaining accuracy of the model. After the training, the so-built PWL-based model can be used for other conditions.

Figure 12 (b) and (c) are the results at $\alpha_0 = 3.0°$ and 2.5° respectively. Not surprisingly, the PWL-model is also valid, since both conditions fall within the training data range. The linear model results are also included for comparison, again unable to capture nonlinear phenomenon at lower angle of attacks.

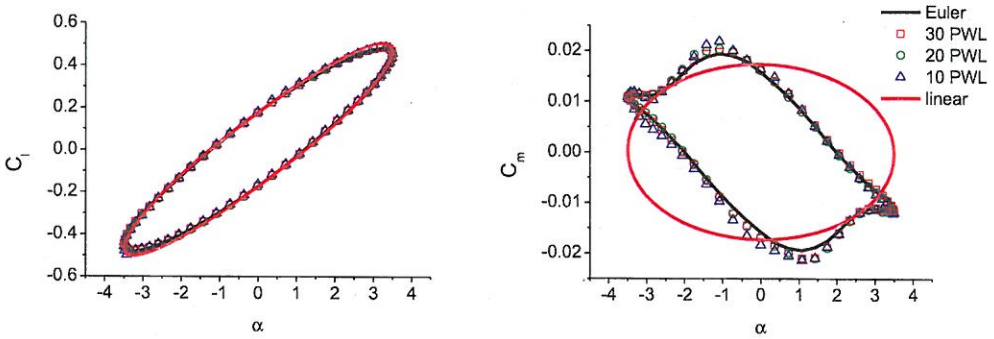

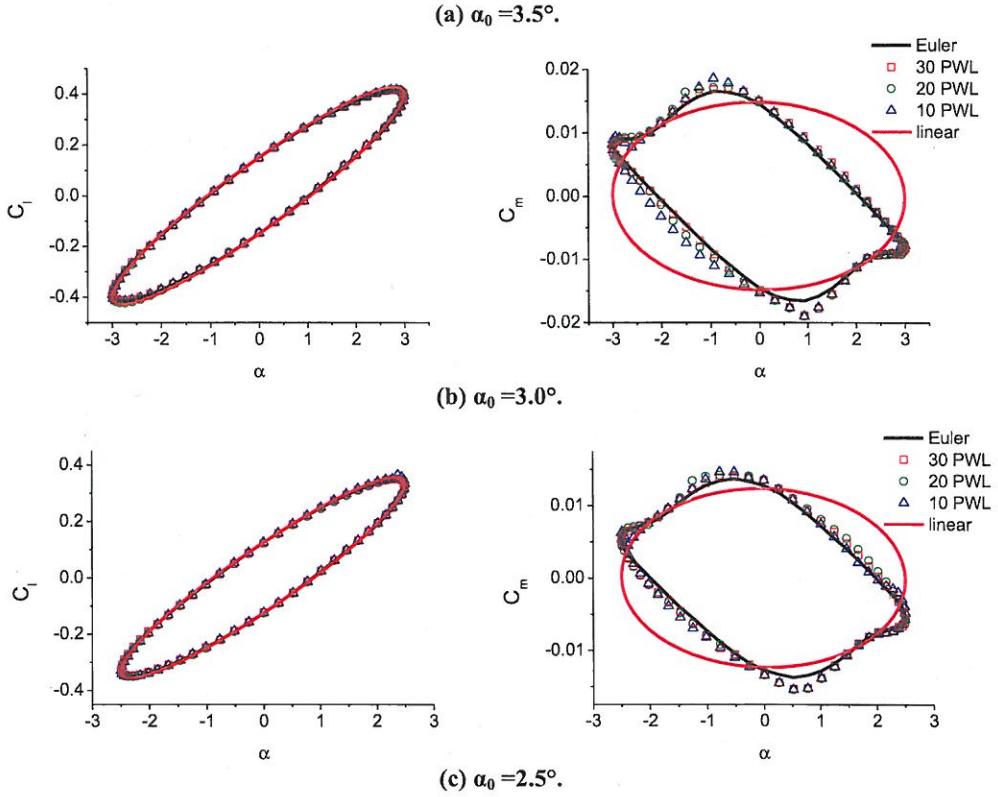

Figure 12. Effects on accuracy by the number of PWL solutions used.

Next there arises a question as to how the model trained for the condition at $\alpha_0 = 3.5°$ and $k = 0.0814$ behaves at different conditions. First, we change the reduced frequency to $k = 0.1$, a 20% larger than the baseline value. Shown in Figure 13, the PWL-model still holds valid. The 10-PWL solution for this case begins to show some noticeable departures from the full solution at the peak Cm, indicating more sample points are needed. It is noted that even though the pitching frequency does not explicitly appear in the formulation, it implicitly affects the flow solution **q**, which in turn changes the residual **R** and related quantities. Obviously, if pitching angle or frequency changes flow structure significantly from those at sample points, then the accuracy of the PWL-model will deteriorate.

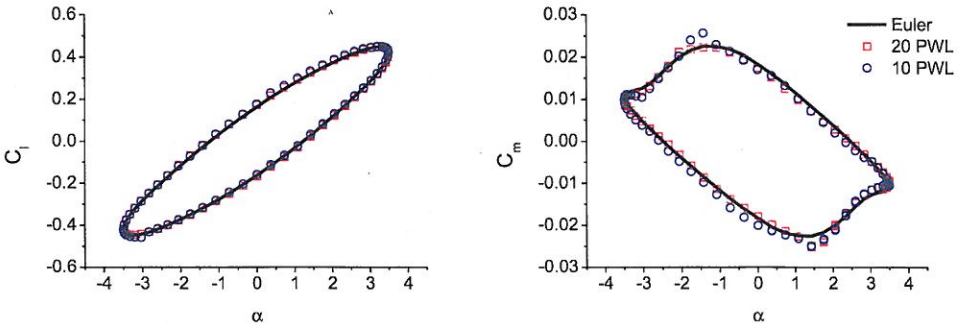

Figure 13. PWL results at different pitching frequency $k = 0.1$ (α_0 =3.5°).

It is also necessary to check if the construction of the solution procedure guarantees convergence. This is tested by decreasing the time step size, in this case by halving the physical time step, $dt = T/120$; results in Figure 14. confirms convergence.

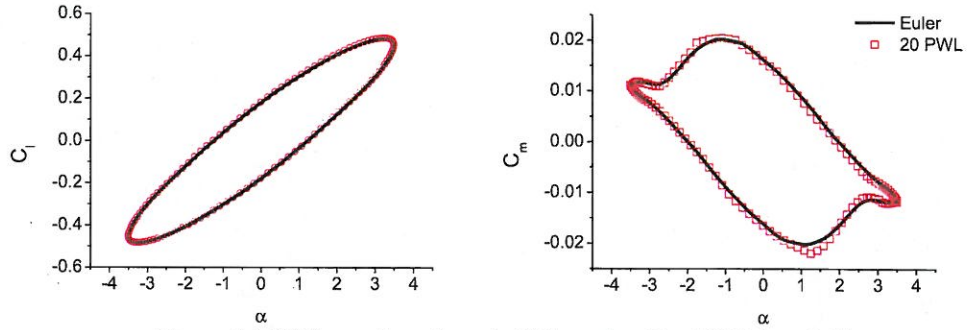

Figure 14. PWL results using a half time step dt = T/120 (α_0 =3.5°).

Now we consider the scenario of having an input, the flight motion, considerably different from the baseline. In this case we impose a cosine signal with the other parameters unchanged.

Figure **15.** shows that the PWL-model is still valid with a different input.

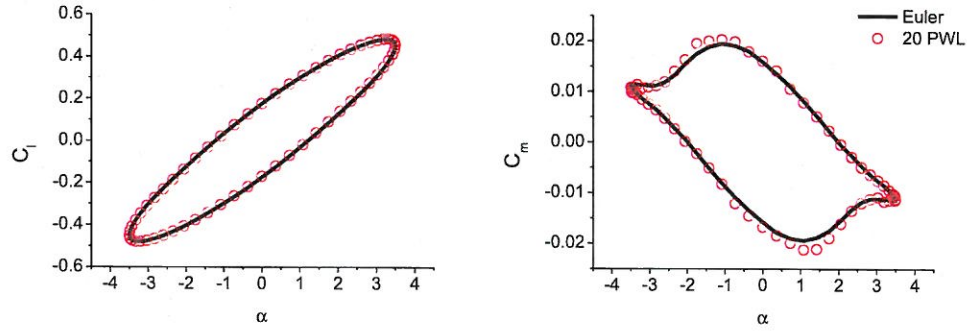

Figure 15. PWL results with cosine signal (α_0 =3.5°, dt = T/60).

With the integrated quantities thoroughly compared, it validates the accuracy of the PWL-based model. It is also interesting to compare the detailed flow structure against the full CFD solution, as shown in Figure 16, and again it confirms the reliability of the present nonlinear model.

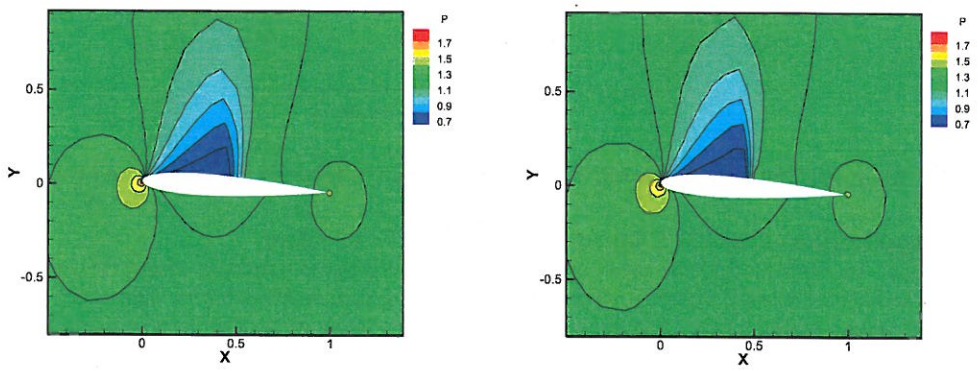

Euler **PWL**

t=T/4

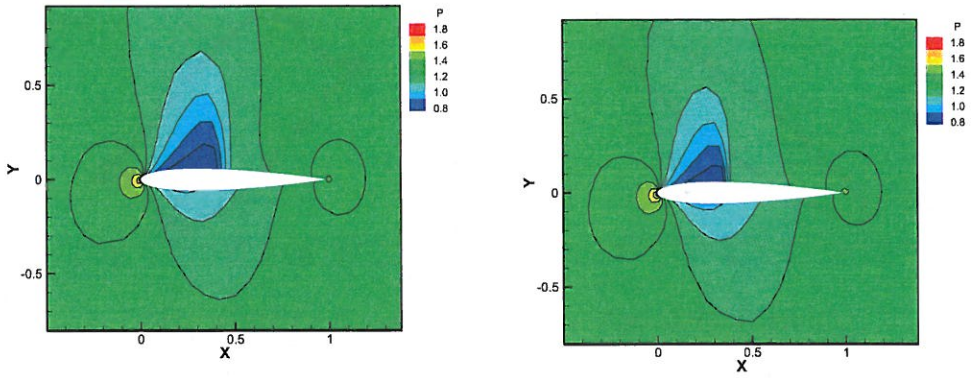

Figure 16. Flow-field expressed by pressure contours at two time slices. cosine signal (α_0 =3.5°, dt = T/60).

Finally, we compare the computational cost for performing a full order CFD analysis and the additional work required to construct the PWL-based nonlinear model, as shown in Figure 17. One should note that this extra overhead is one time only; any computation for other conditions will require a very minimal effort to perform matric-vector multiplications and time integrations, while the full CFD model will be another brand new operations. Hence, in this sense, the so-constructed nonlinear model is not only accurate but also useful for parametric studies and design optimization.

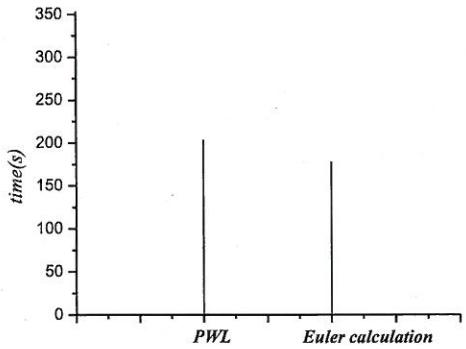

Figure 17. Time consumptions in the full Euler solution and PWL-based modeling (Intel core CPU i7).

B. Further Application of the PWL-based Modeling to CT2 Problem

In this section, we further apply the previously established PWL-based nonlinear model for another unsteady pitching airfoil problem, CT2 in [13]; this problem, while remaining completely subsonic during the entire cycle, is more difficult aerodynamically than CT5 in the sense that the aerodynamic forces display a stronger nonlinearity, as seen in Fig. 8, where the lift force has a noticeable nonlinear behavior near high angle of attack, exhibiting asymmetry in high angles of attack. It is interesting that even at this high angle, the inviscid mechanism is still dominant as validated against the data. The training is carried out at $\alpha_0 = 8^\circ$, again using 20 PWL solutions.

In Figure 18, we show the performance of the PWL-based solutions against the full Euler solutions of different pitching amplitudes. At a small amplitude ($\alpha_0 = 1^\circ$), the flow behaves linearly and the linear model is close to the Euler solution. On the other hand, when the amplitude is only moderate, nonlinearity first appears in the moment

coefficient; then the lift coefficient exhibits a strong nonlinear phenomenon with a double loop, suggesting a second higher-frequency flow structure is embedded in the main flow. The linear model clearly is incapable of following the correct flow behavior.

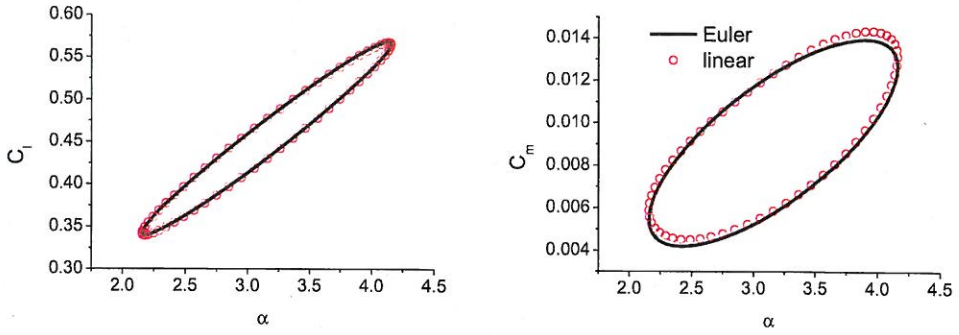

(a) $\alpha_0 = 1°$.

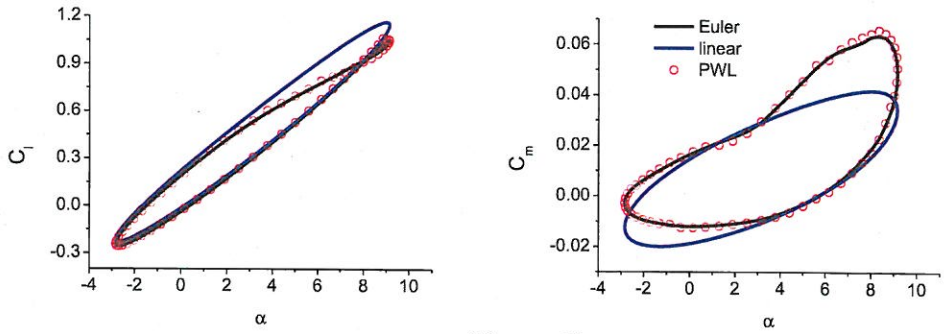

(b) $\alpha_0 = 6°$.

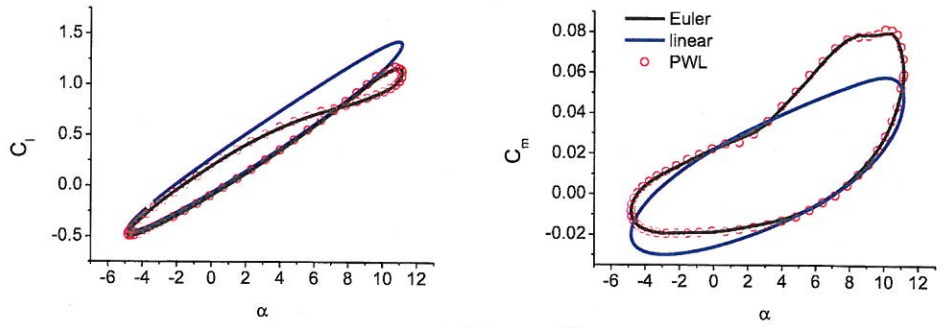

(c) $\alpha_0 = 8°$.

Figure 18. Comparison of Euler, nonlinear PWL-based model and linear solutions of the CT2 airfoil at different pitching amplitudes.

A snapshot of the detailed flowfield is displayed in Figure 19. for a high angle motion ($\alpha_0 = 8°$), showing no discernable differences between the Euler and PWL-based solutions.

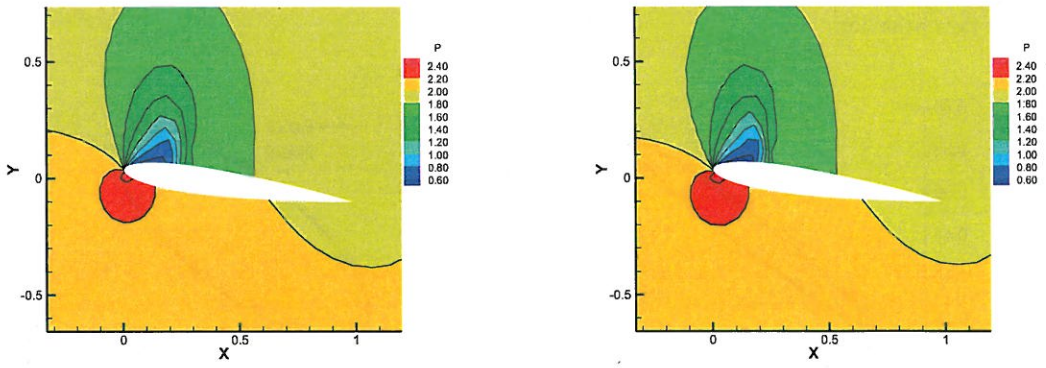

Euler **PWL**

t=T/4

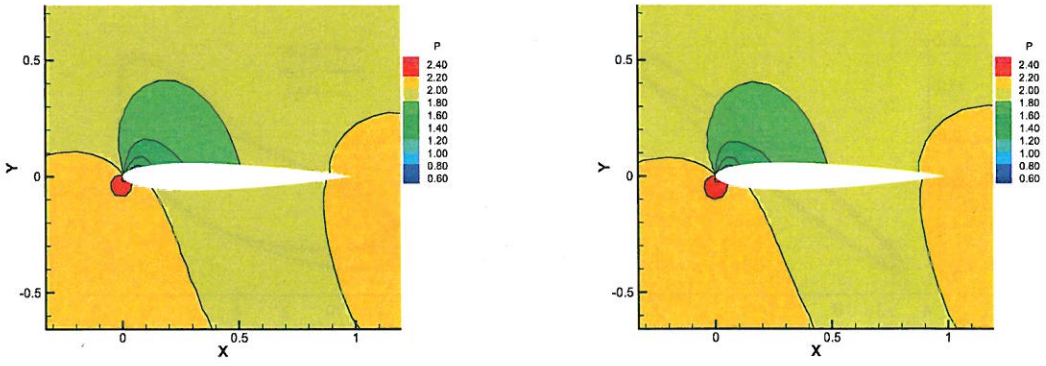

Euler **PWL**

t=T/2

Figure 19. Pressure contours of AGARD CT2 at two time instants (T/4 and T/2) for the airfoil pitching at α_0 = 8°.

Now it is extremely informative to see how the model we constructed performs outside the training trajectory. With the previously-trained model for the trajectory prescribed by Eq. (23) with α_0=8°, and α_m=3.16°, we applied it to a new motion defined by,

$$\alpha = \alpha_m + \alpha_0 \sin^3(2k\tilde{t}) \tag{24}$$

with α_0= 8°, α_m=3.16°, its flight trajectory shown in Figure 20, contains a high (triple) frequency content resulting from the cubic function.

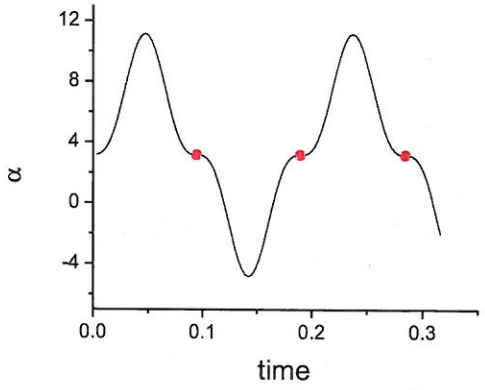

Figure 20. New input trajectory defined in Eq. (24).

A vastly different behavior is revealed in both the lift and moment coefficients, Figure 21 showing sharp discontinuities at the mean angle $\alpha_m = 3.16°$ in both upward and downward phases. The knot point ($\alpha \approx 6°$) in C_l does not find a particularly unusual behavior in C_m. At the mean location, the pitching velocity nearly vanishes, unlike the CT2 motion Eq. (23).

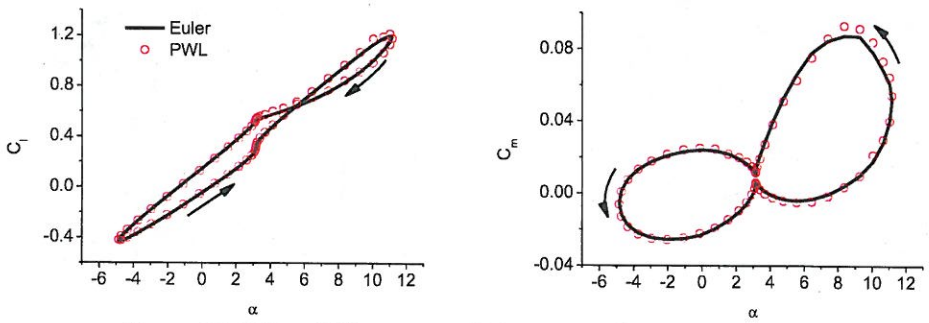

Figure 21. Lift and Moment coefficients responding to Eq. (24) input.

Taking a notch higher by setting $\alpha_0 = 10°$, upward away from the training trajectory, we show the results predicted by the model in Figure 22. Comparing them against the full Euler solution, this case further confirms that the current PWL-based nonlinear model is capable of accurately predicting flowfields considerably beyond the training trajectory, except with some discrepancy near the peak angle.

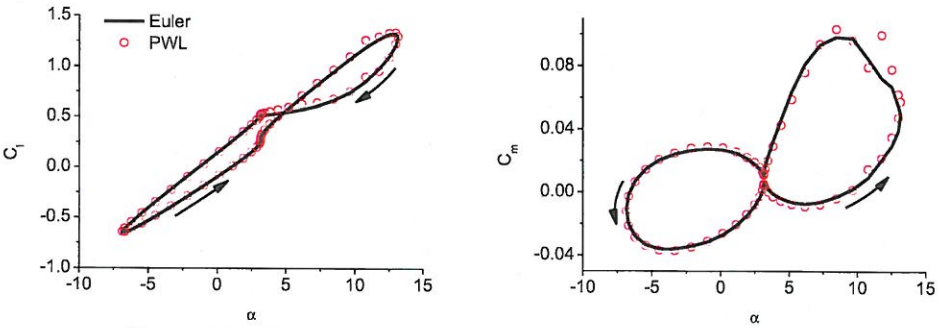

Figure 22. Lift and Moment coefficients responding to Eq. (24) input.

Finally we investigate the flowfield at the knot points, or at the time slices t=T, 3T/2, as shown in Figure 23; the results computed by the model are nearly identical to the CFD results in every detail of the flowfield, also indicating a nonsymmetry here even though the airfoil is at the same angle ($\alpha = 3.16°$) at both times.

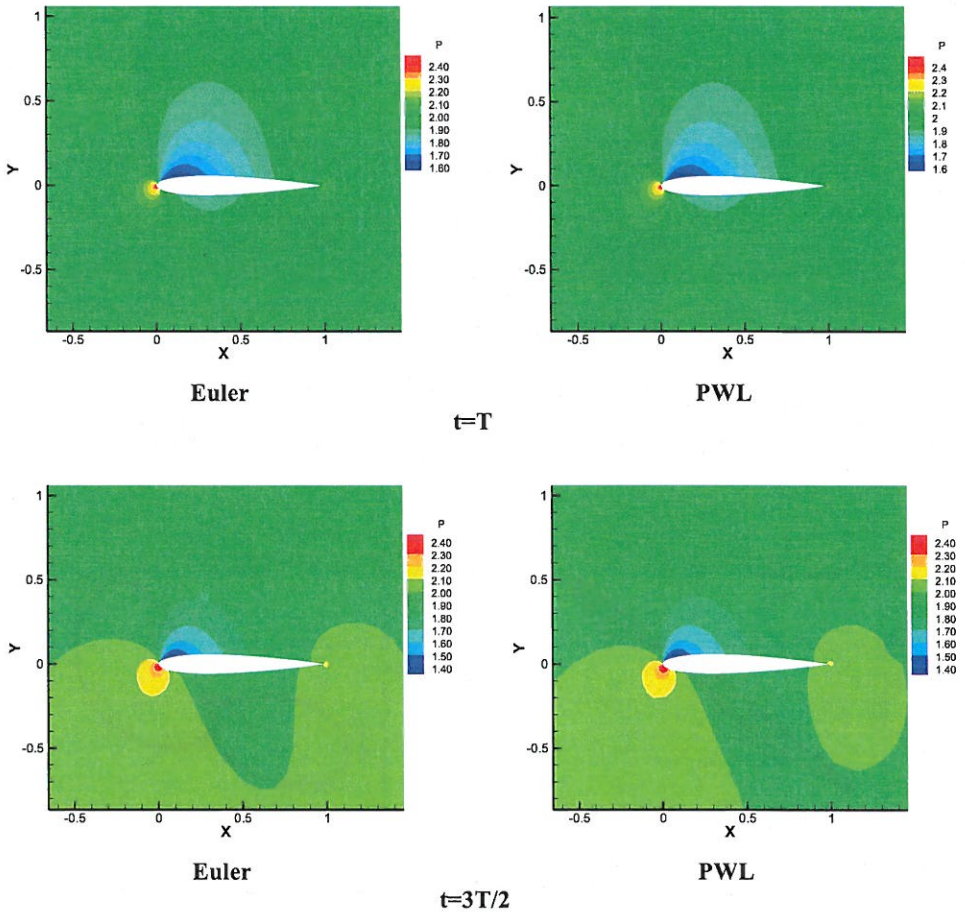

Figure 23. Detailed flowfield by the PWL-based model and CFD, $\alpha_0 = 10°$.

VI. Conclusion

A nonlinear modeling method is proposed by nonlinearly assembling a number of local piecewise linear solutions obtained at some sample points. These points may be defined along the physical or state-variable trajectory, for example simply along the time coordinate in the problems considered in this paper. We show how the piecewise linearization is carried out for the CFD applications. The validity and efficacy of the PWL-based nonlinear model is confirmed first for a scalar equation and subsequently for AGARD test cases, CT2 and CT5; the results shows the accuracy of the model not only for the baseline conditions, but also for conditions beyond the training trajectory. The nonlinear characteristics in the flowfield and aerodynamic forces with respect to the varying angle of attack are predicted in close agreement with the full Euler model. The model is capable of predicting the flowfield accurately in response to an input that is vastly differently from the baseline, yielding a flow structure not existing in the baseline solution. The accuracy, robustness, and efficiency of the model constructed by the proposed method suggest that the method can be valuable for the situations where repeated computations are required for a host of input and parameters changes, such as design optimization.

To further reduce the computation cost for preparing the PWL-based model, some model reduction techniques by projection onto a much smaller subspace, such as balanced truncation, has been implemented and the results will be presented elsewhere.

Acknowledgments

This research was supported by the Subsonic Fixed Wing Project, under NASA's Fundamental Aeronautics Program.

References

[1]Rewienski, M. and White, J. "Improving trajectory piecewise-linear approach to nonlinear model order reduction for micro-machine devices using an aggregated projection basis," *IEEE Trans. on Computer-Aided Design of Integrated Circuits and System*, Vol. 24, No. 2, 2003, pp. 155-170.

[2]Beran. P.S, Lucia. D.J, and Pettit. C.L, "Reduced-order modeling of limit-cycle oscillation for aero-elastic systems," *J. Fluid and Structures*, Vol. 19,No. 5, 2004, pp. 575-590.

[3]Moore. B.C, "Principle component analysis in linear system controllability, observability, and model reduction", *IEEE Automat. Control*, Vol. 26, No. 1, 1981, pp. 17-32.

[4]Laub, A.J., Heath, M.T., Page, C.C., Ward, R. C., "Computation of system balancing transformations and other applications of simultaneous diagonalization algorithms," *IEEE Trans, Automat. Control.* Vol. 32, No. 2, 1987, pp. 115-122.

[5]Willcox.K., and Peraire,J., "Balance model reduction via the proper orthogonal decompostion", *AIAA Journal*, Vol. 40, No. 11, 2002, pp. 2323-2330.

[6]Rowely, C.W., "Model reduction for fluids using balanced proper orthogonal decomposition," *Int. J. Bifurcation Chaos*, Vol. 15, No. 3, 2005, pp. 997-1013.

[7]Gu, C. and Roychowdhury, J., "Model reduction via projection onto nonlinear manifolds with application to analog circuits and biochemical systems," *IEEE/ACM International Conference on Computer-Aided Design*, 2008, pp. 85-92.

[8]Gratton, D. and Willcox, K., "Reduced-order, trajectory piecewise-linear models for nonlinear computational fluid dynamics", *34th AIAA Fluid Dynamics Conference and Exhibit,* AIAA 2004-2329.

[9]Jesmani, M., Hosseini, B. and Chalaturnyk, R., "Use of streamlines in development and application of a linearized reduced-order reservoir model," *9th International Geostatistics Congress*, 2012.

[10]Yao, W. and Liou, M.-S., "Reduced-order modeling for flutter/LCO using recurrent artificial neural network", *14th AIAA/ISSMO Multidisciplinary Analysis and Optimization Conference*, AIAA 2012-5446.

[11]Glaz, B., Liu, L., and Friedmann, P., "Reduced-order nonlinear unsteady aerodynamic modeling using a surrogate-based recurrence framework," *AIAA J.* Vol. 48, No. 10, 2010, pp. 2418-2429

[12]Liou, M.-S., "A sequel to AUSM, Part II: AUSM+-up" *J. Comput. Phys.*, Vol. 214, No. 1, 2006, pp. 137-170.

[13]AGARD, "Compendium of unsteady aerodynamic measurements," AGARD-R-702, 1982.